TERRAIN DEFORMATION MODELING BY PHOTOGRAMMETRIC EXPLOITATION OF HIGH-RESOLUTION SATELLITE IMAGERY

Chunsun Zhang, Associate Professor
Geographic Information Science Center of Excellence (GIScCE)
South Dakota State University
1021 Medary Ave, Brookings SD 57007, USA
chunsun.zhang@sdstate.edu

Michael P. Crane, Associate Land Sciences Team Manager
EROS Data Center, U.S. Geological Survey
Sioux Falls, SD 57198, USA
mpcrane@usgs.gov

Clive Fraser, Professor
Department of Geomatics, The University of Melbourne
Parkville, VIC 3010, Australia
c.fraser@unimelb.edu.au

ABSTRACT

Terrain deformation data is utilized in many applications including geological hazard monitoring and modeling. In particular, these data play an important role in tectonic deformation modeling and are being used to study the coseismic and postseismic processes of the 2004/2005 earthquake events associated with the Sumatra-Andaman Subduction Zone (SASZ). Terrain deformation is usually assessed by the comparison of digital surface models (DSM) of the terrain acquired pre and post event. While new technologies such as lidar are available for almost instant DSM generation, the use of stereoscopic high-resolution satellite imagery, coupled with image matching, affords cost-effective measurement of surface topography over large geographic areas. This investigation explores the potential of high-resolution stereo imagery for producing DSMs in SASZ using a bias-corrected rational polynomial coefficients (RPCs) sensor orientation model and a hybrid image-matching algorithm. We show in the paper that the bias-corrected RPCs model allows for sub-pixel geopositioning accuracy over a large area, even with few ground control points. The DSMs are automatically generated by an improved image matching approach. The approach involves an integration of feature point, grid point and edge matching algorithms. It makes use of explicit knowledge of the image geometry and employs a coarse-to-fine hierarchical strategy. The DSMs are generated by a combination of matching results of feature points, grid points and edges. Following DSM generation, orthoimages are produced. Accuracies of the DSM and the orthoimages as assessed using checkpoints are reported to validate the feasibility of our method for terrain deformation modeling in the SASZ.

INTRODUCTION

The devastating 2004 M9 and 2005 M8.7 earthquakes in the SumatraAndaman Subduction Zone (SASZ), ruptured a 1200-kilometer length of the boundary where the Eurasian Plate overrides the Indo-Australian Plate. The resultant vertical and horizontal deformation to the seafloor and surrounding land surfaces has created a natural laboratory for testing and evaluating state-of-the-art remote sensing techniques for characterizing temporal change in the landscape. These techniques will yield quantitative measurements of the horizontal and vertical displacement for use in constraining finite element models (FEMs) to improve their numerical simulations.

Terrain deformation can be assessed by the comparison of DSMs acquired pre and post event. While Light Detection and Ranging (LIDAR) and Interferometric Synthetic Aperture Radar (IFSAR) techniques can produce topographic information, photogrammetry has been and remains a most effective technique for accurate DSM production. In particular, the recent introduction of high-resolution satellite imagery (HRSI) systems such as IKONOS

and QuickBird have initiated a new era of Earth observation and digital mapping. In addition to offering high-resolution and multispectral data, these systems provide a short revisit capability and can perform stereo mapping. In particular, imagery collected from high-resolution satellite sensors can alleviate temporal variability concerns as the tens-of-seconds separation between in-track stereo image capture allows consistent imaging conditions, thus increasing the likelihood of image matching success. These superior characteristics make HRSI well suited for DSM generation (Toutin, 2004; Zhang, 2005; Poon et al., 2005; Krauss et al., 2005; Sohn et al., 2005; Zhang and Gruen, 2006; Poon et al., 2007) and feature extraction (Hu and Tao, 2003; Di et al., 2003; Zhang et al., 2005). This paper explores the utility of IKONOS Geo stereo imagery for generating accurate digital surface models in remote areas with very limited ground control to support tectonic deformation modeling.

SENSOR MODELING AND IMAGE ORIENTATION

The IKONOS satellite operates with a linear array scanner where images are obtained with a pushbroom sensor. Thus, the imagery is composed of consecutive scan lines where each line is independently acquired and has its own time dependent attitude angles and perspective centre position. To describe mathematically the object-to-image space transformation, the rational polynomial coefficient (RPC) model has been universally accepted and extensively used (Baltsavias et al., 2001; Jacobsen, 2003; Grodecki and Dial, 2003; Fraser et al., 2002; Fraser and Hanley, 2003; Poli, 2004; Eisenbeiss et al., 2004). RPCs are derived from a rigorous sensor model (Grodecki and Dial, 2003) and supplied with the imagery. The general form of the model is described as:

$$l = l_n L_S + L_0, \;\; s = s_n S_S + S_0 \tag{1}$$

$$l_n = \frac{Num_L(U,V,W)}{Den_L(U,V,W)}, \;\; s_n = \frac{Num_S(U,V,W)}{Den_S(U,V,W)} \tag{2}$$

where

$$Num = \sum_{i=0}^{3}\sum_{j=0}^{3}\sum_{k=0}^{3} a_{ijk} U^i V^j W^k \;,\; Den = \sum_{i=0}^{3}\sum_{j=0}^{3}\sum_{k=0}^{3} b_{ijk} U^i V^j W^k \tag{3}$$

and l_n and s_n are the normalized line and sample coordinates, with L_S and L_0 the line scale and line offset, S_S and S_0 the sample scale and sample offset. *U*, *V* and *W* are the normalized latitude, longitude and ellipsoidal height.

Because RPCs are derived from orientation data originating from the satellite ephemeris and star tracker observations, without reference to ground control points (GCPs), they can give rise to geopositioning biases. These biases can be accounted for by introducing additional parameters (Fraser and Hanley, 2003; Fraser et al., 2006). The practical bias compensated model can be written as:

$$\begin{aligned} l + A_0 + A_1 l + A_2 s &= \frac{Num_L(U,V,W)}{Den_L(U,V,W)} L_S + L_0 \\ s + B_0 + B_1 l + B_2 s &= \frac{Num_S(U,V,W)}{Den_S(U,V,W)} S_S + S_0 \end{aligned} \tag{4}$$

Here, A_0, A_1, $A2$, B_0, B_1, B_2 are the image affine distortion parameters for bias compensation. After the bias compensation process, bias-corrected RPCs can be generated by incorporating bias compensation parameters into the original RPCs, allowing bias-free application of RPC positioning without the need to refer to additional correction terms (Fraser and Hanley, 2003; Grodecki and Dial, 2003; Fraser et al., 2006). It has been shown in previous research that with bias-corrected RPCs, 1 pixel level geopositioning accuracy can be achieved from high-resolution satellite imagery (Dial and Grodecki, 2002a; Fraser and Hanley, 2003; Fraser and Hanley, 2005; Baltsavias et al., 2005; Fraser et al., 2006). As demonstrated in Dial and Grodecki (2002b), sub-pixel accuracy is usually obtained from IKONOS image strips of shorter than 50km in length.

DIGITAL SURFACE MODEL GENERATION

Image matching has been an active topic in photogrammetry and computer vision for decades. The goal of image matching is to automatically find the correspondences on overlapping images, thus it is a critical technique in many applications, including digital surface model generation. A wide variety of approaches have been developed for DSM generation via image matching and many have been implemented in commercially available photogrammetric systems. However, a fully automatic, precise and reliable image matching method adaptable to various different images and scene contents is still to be developed. The limitations arise mainly from an insufficient understanding and modeling of the underlying process and a lack of appropriate theoretical measures for self-tuning and quality control. The difficulty of image matching comes from, for example radiometric distortion, geometric distortion, occlusions, repeated patterns and lack of features.

We have developed an image matching approach for automatic DSM generation from high-resolution satellite images, which has the ability to provide dense, precise, and reliable results. The approach uses a coarse-to-fine hierarchical strategy with several image matching algorithms, essentially combining the matching results of the feature points, grid points and edges. The general scheme is outlined in Fig. 1.

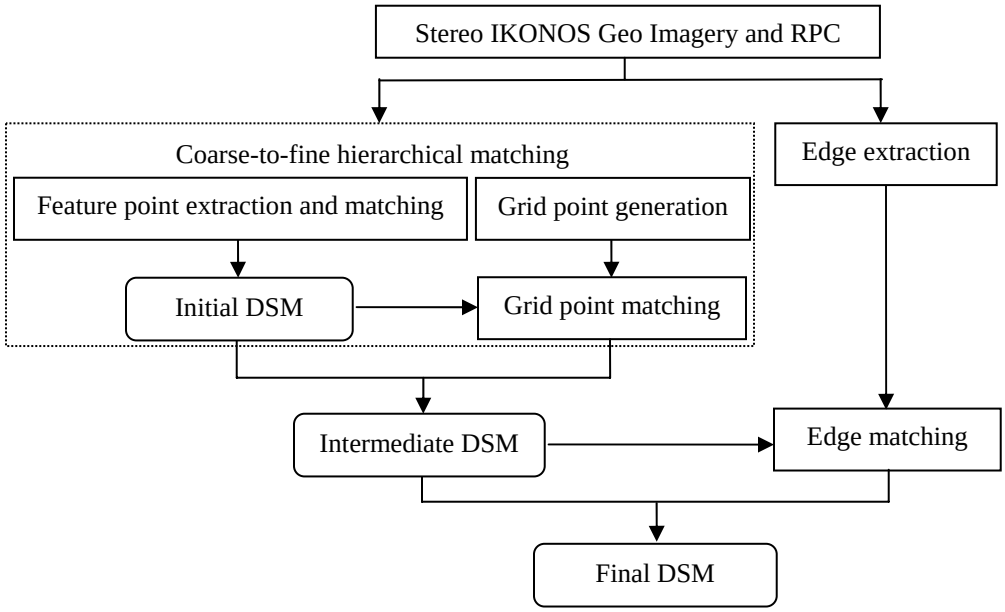

Figure 1. General scheme of image matching for DSM generation from high-resolution satellite imagery.

The coarse-to-fine hierarchical strategy necessarily involves image matching following an image pyramid approach. That is, the solution of correspondences is found from the top of the image pyramid progressively to the bottom of the pyramid, the image of the original resolution. During the process, the result from a higher level of the pyramid is used as an approximation and adaptive computation of the matching parameters at the subsequent lower level. Matching continues until the lowest level of the pyramid is reached, where the highest accuracy results are also obtained. In addition, the DSM is first generated from the feature points, progressively incorporating more features such as grid points and image edges. Again, as in the image pyramid approach, the resulting DSM from previous feature matching serves as a guide in matching successive features, while the DSM itself will be augmented with the new features, resulting in a dense DSM which allows for better characterization of the terrain.

Feature Point Matching

Our feature point matching method exploits image pixel grey value similarity and geometrical structure information. The image matching is performed in two steps, where different matching algorithms are employed at each step. The method starts with image enhancement and feature point extraction. Candidate conjugate points are then located by cross correlation in which the normalized correlation coefficient is used for the similarity measure. This information is then used as prior information in the next step, structural matching. The locally consistent matching is

achieved through structural matching with probability relaxation (Zhang and Fraser, 2007).

We applied a new version of the Wallis filter (Baltsavias, 1991) to optimize the images for subsequent image matching. This filter enhances features in images and therefore enables improved feature point extraction. Furthermore, since the filter is applied in both images using the same parameters, naturally occurring brightness and contrast differences are corrected. Following the image enhancement process, feature points are extracted using the well-known Foerstner operator.

The normalized cross-correlation coefficient forms the similarity measure of the candidate matching areas. This measure has been shown to be largely independent of differences in brightness and contrast due to normalization with respect to the mean and standard deviation. If (x, y) and (x', y') are the image coordinates of two feature points located in images f and g, the normalized cross-correlation in a $(2N+1)*(2N+1)$ window is given as

$$\rho = \frac{C_{fg}}{\sqrt{C_{ff} * C_{gg}}} \tag{5}$$

where

$$C_{fg} = \sum_{i=-N}^{N}\sum_{j=-N}^{N}(f(x-i,y-j)-\overline{f})(g(x'-i,y'-j)-\overline{g}) \tag{6}$$

$$C_{ff} = \sum_{i=-N}^{N}\sum_{j=-N}^{N}(f(x-i,y-j)-\overline{f})^2 \tag{7}$$

$$C_{gg} = \sum_{i=-N}^{N}\sum_{j=-N}^{N}(g(x'-i,y'-j)-\overline{g})^2 \tag{8}$$

and $\overline{f}$ and $\overline{g}$ are the local means of the windows in images f and g, respectively.

A matching pool for candidate conjugate points is constructed with the computed similarity measures and a similarity score is attached to each candidate point pair. Although the correlation coefficient is a good indicator of the similarity between points, problems still exist in determining all correct matches. Firstly, there is the difficulty of how to decide on a threshold in correlation coefficients to select the correct matches. The existence of image noise, shadows, occlusions, and repeated patterns exacerbates this problem. Furthermore, matching using a very local comparison of grey value difference does not necessarily always deliver consistent results in a local neighbourhood. In order to overcome these problems, the structural matching algorithm with probability relaxation proposed in Zhang and Baltsavias (2000) has been adopted here.

Let the feature points in the first image be a set L, $L=\{l_i\}$, $i=1, 2, \ldots n$, and the feature points in the second image be a set R, $R=\{r_j\}$, $j=1,2,\ldots m$. The mapping from the first image to the second image is represented as T. Assuming the right type of mapping T, we seek the probability that l_i matches r_j, i.e. the matching problem becomes the computation of a conditional probability $p\{\ l_i = r_j \mid \mathrm{T}\}$ (the '=' sign means 'match to'). The computation of the conditional probability is via an iterative scheme (Christmas et al., 1995; Zhang and Baltsavias, 2000; Zhang and Gruen, 2006):

$$p^{(t+1)}\{l_i = r_j \mid T\} = \frac{p^{(t)}\{l_i = r_j\}Q^{(t)}(l_i = r_j)}{\sum_{r_h \in R} p^{(t)}\{l_i = r_h\}Q^{(t)}(l_i = r_h)} \tag{9}$$

where

$$Q^{(t)}(l_i = r_j) = \prod_{h=1,h\neq i}^{n}\sum_{k=1}^{m} C\{T(l_i, rj\ ; l_h, r_k) \mid l_i = r_j, l_h = r_k\}p^{(t)}\{l_h = r_k\} \tag{10}$$

The value of Q expresses the support that is given to the hypothesis match ($l_i = r_j$) from neighbouring points taking into consideration the relations between them.

The function $C\{T(l_i, rj\ ; l_h, r_k) \mid l_i = r_j, l_h = r_k\}$ is called the "compatibility function". Its value is in the range between 0 and 1, quantifying the compatibility between the match ($l_i = r_j$) and a neighbouring match ($l_h = r_k$). The compatibility function plays an important role in the process of structural matching. In this investigation, we adapted

the function defined in Zhang and Gruen (2004) as

$$
\begin{aligned}
& TI / \exp(\Delta p_x^2 + \Delta p_x^2) / k) \\
& \Delta p_x = (x_h - x_i) - (x_k - x_j) \\
& \Delta p_y = (y_h - y_i) - (y_k - y_j)
\end{aligned}
\tag{11}
$$

Here, *k* is a constant and the parameter *TI* is quantified by the texture information. Its value is obtained from the average correlation coefficient values for the point pairs (*i, j*) and (*h, k*). In addition to the image texture information, this definition of the compatibility function also takes into account the geometric relations. The iteration scheme is then initialised by assigning the previously computed normalized correlation coefficient to $p^{(0)}\{l_i = r_j\}$ for a possible matched pair l_i and r_j. This will increase matching success while reducing computation cost and time. When the iterative procedure is terminated, the point pair that receives the highest probability is selected as the actual match.

Grid Point Matching

Feature points often exist in texture-rich regions, and correspond to points at places with grey value variation. These points are usually suitable for accurate and reliable matching. In case of image regions with poor texture or no texture information, few or even no feature points can be extracted. The image matching with only feature points will leave holes on the DSM in these areas. To solve this problem, grid points can be used and grid point matching will be conducted (Hsia and Newton, 1999; Gruen and Zhang, 2005; Zhang, 2005; Baltsavias et al., 2005). Grid points are determined at given positions, uniformly distributed over the whole image. As for feature points, the grid points are matched using cross-correlation and structural matching with epipolar constraint following the coarse-to-fine concept. Since grid points may lie in regions with poor texture, shadows or occlusions, the search for the match of a grid point has a higher possibility to yield ambiguity or no matching candidate. To increase the reliability of the grid point matching, the DSM generated from feature point matching is employed to constrain the matching candidate search. This will further reduce the search space and thus decrease ambiguity while speeding up the matching process.

Edge Matching

The edge extraction and matching algorithms developed in Zhang and Baltsavias (2000) are adopted in our work. This method was developed for automated 3D reconstruction of man-made objects from airborne and spaceborne images (Zhang, 2003; Baltsavias and Zhang, 2005). The method exploits rich edge attributes and edge geometrical structure information. The rich edge attributes include the geometrical description of the edge and the photometric information in the regions immediately adjacent to the edge. The epipolar constraint is applied to reduce the search space. The similarity measure for an edge pair is computed by comparing the edge attributes. The similarity measure is then used as prior information in structural matching. The locally consistent matching is achieved through structural matching with probability relaxation. More details of the matching strategy can be found in Zhang and Baltsavias (2000) and Zhang (2003).

Edges are extracted using the Canny operator and then fitted to generate straight lines. For each straight edge segment, we compute the position, length, orientation and robust photometric statistics for the left and right flanking regions. The photometric properties include the median and the scatter matrix.

The epipolar constraint is employed to reduce the search space. The two end points of an edge segment in one image generate two epipolar lines in the other image. With the approximated height information derived from feature point and grid point matching, an epipolar band of limited length is defined. Any edge included in this band (even partially) is a possible candidate. The comparison with each candidate edge is then made only in the common overlap length, i.e. ignoring length differences and shifts between edge segments. For each pair of edges that satisfy the epipolar constraints above, their rich attributes are used to compute a similarity score. Therefore, the similarity score is a weighted combination of various criteria. The detailed computation can be found in Zhang and Baltsavias (2000).

After the computation of similarity measurement, we construct a matching pool and attach a similarity score to each candidate edge pair. Since matching using a local comparison of edge attributes does not always deliver correct results, the structural matching using probability relaxation, similar to that in point matching, are conducted. The

method seeks the probability that an edge in one image matches an edge in the other image, using the geometrical structure information and photometric information of neighboring image edges. Therefore, the correspondences of both individual edges and edge structures are found. As in point matching, the computed edge similarity scores are used as prior information in structural matching. The compatibility function is evaluated using the differences between the relational measurements of two edge pairs in the stereo images. Zhang and Baltsavias (2000) and Zhang (2003) give further details of the definition of relational measurements and provide an evaluation of the compatibility function.

EXPERIMENT RESULTS

The datasets that will be used in this project consist of Digital Globe and IKONOS Geo imagery stereo scenes for five study sites in the Andaman/Nicobar Islands of the Indian Ocean. Weather conditions in this tropical study area are making it difficult to acquire cloud free imagery. Therefore, to test and evaluate the developed algorithms, we applied the matching approach to a set of along track stereo IKONOS Geo images for Hobart, Australia in order to extract a DSM. This scene encompasses a total area of 120 km^2 and encompasses a variety of land cover types, including mountainous forest (to a height of 1200 m above sea level), hilly suburban neighbourhoods, parks, urban housing and commercial buildings (Fig. 2). The images were acquired towards the end of the southern hemisphere summer season. Note the cloud cover in the lower left side of the Fig. 1. A more complete description of the scene can be found in Fraser and Hanley (2005).

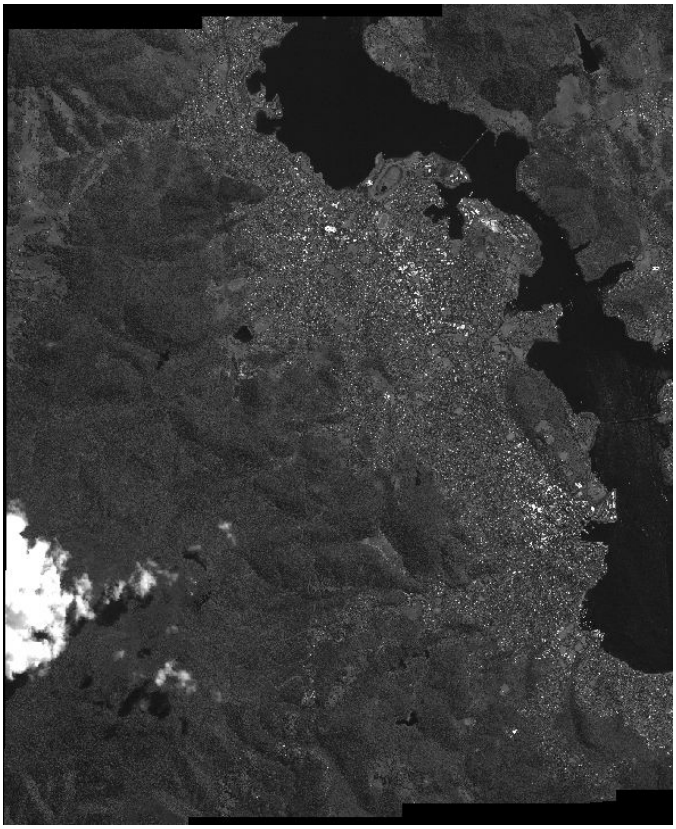

Figure 2. IKONOS image of Hobart, Australia.

The vendor-supplied RPCs were refined with the bias compensation model using ground control points. This process corrected the bias in the original RPCs and improved the geopositioning accuracy. The effectiveness of this process is demonstrated in Fig. 3 where the center of a roundabout with GPS-surveyed coordinates is projected to the image space using the vendor-supplied RPCs (left) and the bias-corrected RPCs (right). Due to the bias in the original

RPC, the projected center deviates from its correct position. With the bias-corrected RPCs, the discrepancy is removed, and the projected center accurately coincides with the center of the roundabout in image space.

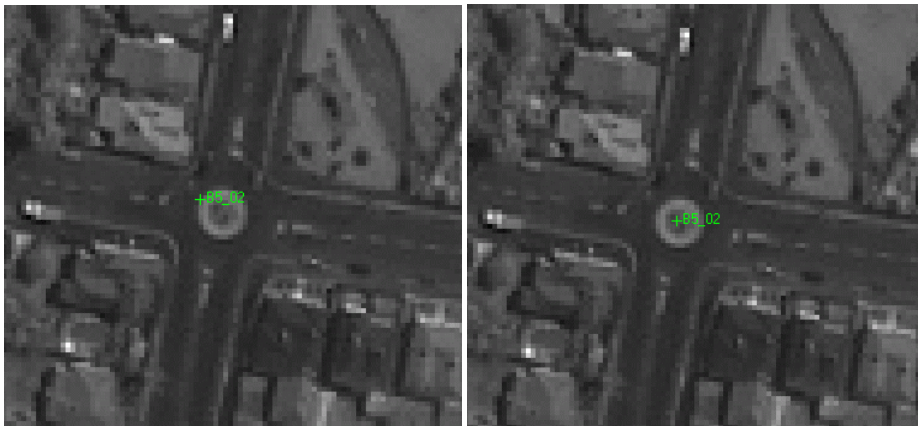

Figure 3. The center of a roundabout with GPS-surveyed ground coordinates was projected to image space using vendor-supplied RPCs (left) and bias-corrected RPCs (right).

The bias-corrected RPCs are then used in image matching for DSM extraction. The process began with feature point matching, and the DSM was progressively augmented with the results from grid matching and edge matching. In total, nearly 7 million conjugates points were finally located. The matched points and edges were transformed to 3D object space through space intersection using the forward RPC model. The DSM generated with 5m grid spacing is illustrated in Fig. 4. Visual inspection reveals that good results have been achieved. The very dense terrain points enable delineation of the terrain in more detail. By combining results of multi feature matching, particularly the edge features, the fine structures of the terrain including streets, large buildings and other infrastructure are also modeled. Unfortunately, reference data is lacking for this region, so quantitative evaluation of the results was made using only GPS-surveyed ground check points. This point-based comparison reveals that a height discrepancy of about 1m has been achieved. However, this evaluation represents optimal conditions at check points which are easily identifiable, highly contrasted in the image and located in locally flat areas.

DISCUSSION AND CONCLUSION

This paper has presented a scheme for modeling tectonic deformation using high-resolution satellite imagery in support of the study of coseismic and postseismic processes of earthquake events. Key components presented are methods to explore IKONOS Geo stereo imagery for producing dense and detailed DSMs over large areas. First, the vendor-supplied sensor model coefficients must be refined using a bias compensation model to achieve sub-pixel geopositioning accuracy. The approach is quite effective and requires very limited ground control points. This is an advantage, and it is especially beneficial in remote areas such as the SASZ where collection of GCPs is difficult. Then the DSM is automatically generated by an improved image matching algorithm using the bias-corrected RPCs. The matching approach involves an integration of feature point, grid point and edge matching algorithms, makes use of explicit knowledge of the image geometry and works in a coarse-to-fine hierarchical strategy. The coarse-to-fine strategy allows for the matching process following an image pyramid approach, while progressively reconstructing the terrain model from feature points, grid points to edges. This strategy reduces search space, provides more reliable results, and speeds up the process. For the matching of each feature, a two-step scheme is employed in which the candidates are first found using normalized correlation coefficient (for points) or by comparing attributes (for edges), while the final matches are located by a structural matching algorithm. This scheme avoids a hard threshold in deciding matches which usually causes commission and omission errors, while providing locally consistent results in a neighborhood. The integration of multi features for DSM generation is another advantage of the proposed approach. The grid point matching allows for bridging gaps or holes in regions with poor or no texture. The integration of edges in the DSM is particularly useful and preserves the discontinuity of the terrain as demonstrated in the experimental

results. This process has been used to generate a DSM with very dense points over a large area that allows for better characterization of terrain, thereby benefiting terrain deformation modeling.

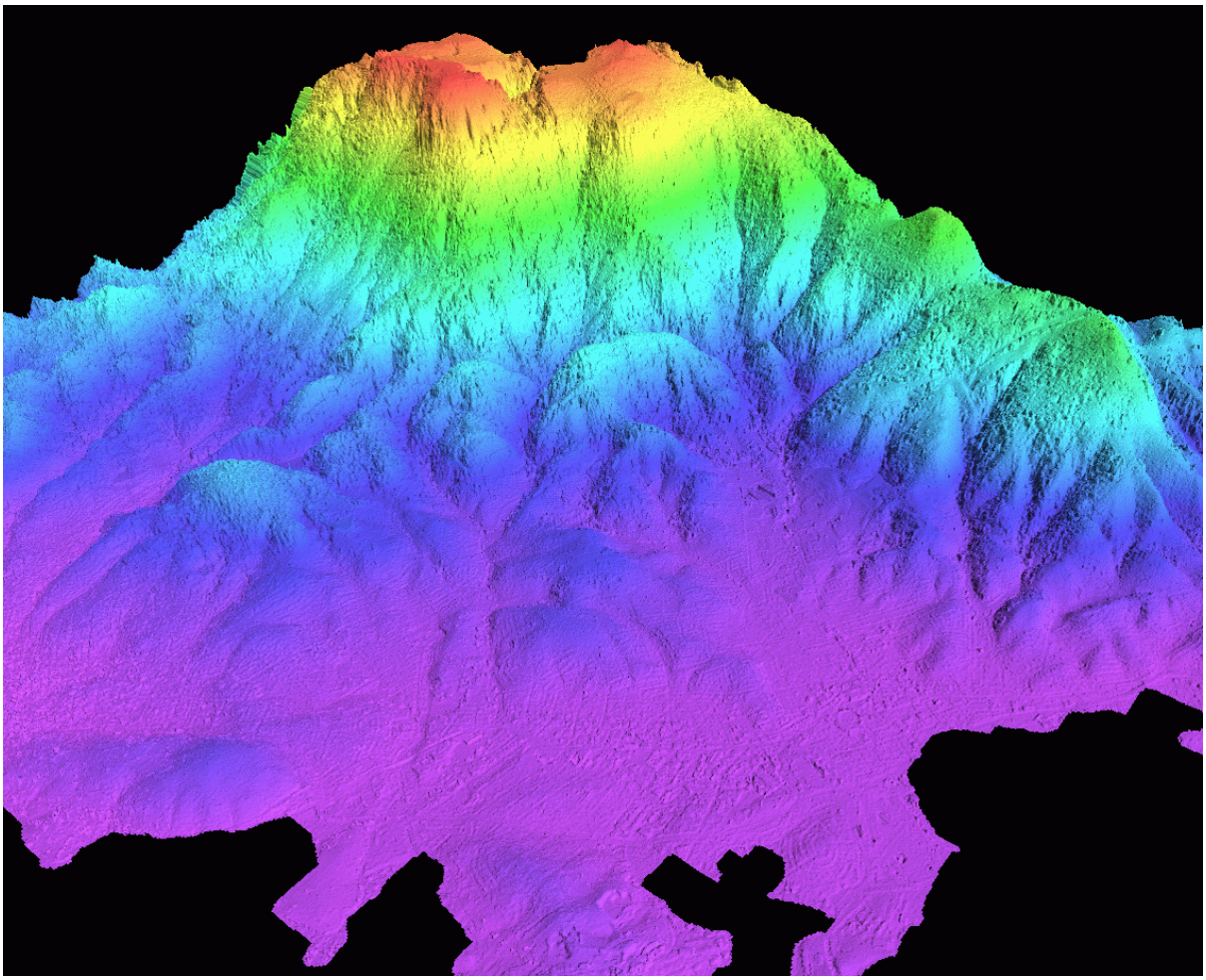

Figure 4. Extracted digital surface model from IKONOS Geo imagery over Hobart, Australia.

ACKNOWLEDGEMENTS

The work described in this paper is partially supported by the U.S. Geological Survey.

REFERENCES

(IAPRSSIS = International Archives of Photogrammetry, Remote Sensing and Spatial Information Science)

Baltsavias, E. P. (1991). Multiphoto geometrically constrained matching. *PhD Dissertation, Report No. 49*, Institute of Geodesy and Photogrammetry, ETH Zurich, Switzerland. 221 pages.

Baltsavias, E. P., M. Pateraki, and L. Zhang (2001). Radiometric and geometric evaluation of IKONOS Geo images and their use for 3D building modeling. *Joint ISPRS Workshop on "High Resolution Mapping from Space 2001"*, Hannover, Germany, 19-21 September. CD-ROM.

Baltsavias, E. P., L. Zhang, and H. Eisenbeiss (2005). DSM generation and interior orientation determination of IKONOS images using a testfiled in Switzerland. *IAPRSSIS* 36, (Part I/W3). CDROM.

Baltsavias, E.P. and C. Zhang, (2005). Automated updating of road databases from aerial images. *International Journal of Applied Earth Observation and Geoinformation*, *6*(3-4):199-213.

Di, K., R. Ma, and R. Li (2003). Automatic shoreline extraction from high-resolution IKONOS satellite imagery. Proc. of ASPRS 2003 Conference, Anchorage, Alaska, May 5-9. CDROM.

Dial, G., and J. Grodecki (2002a). RPC replacement camera models. *IAPRSSIS*, Vol, 34, Part XXX. CDROM.

Dial, G., and J. Grodecki (2002b). Block adjustment with rational polynomial camera models. Proc. of ASPRS Annual Conference, Washington, DC, 22-26 May. CDROM.

Dial, G., and Grodecki, J. (2002c). IKONOS accuracy without ground control *IAPRSSIS*, 34(1). CDROM.

Eisenbeiss, H., E. P. Baltsavias, M. Pateraki, and L. Zhang (2004). Potential of IKONOS and QUICKBIRD imagery for accurate 3D-Point positioning, orthoimage and DSM generation. *IAPRSSIS*, *35* (B3): 522-528.

Fraser, C., E. P. Baltsavias, and A. Gruen (2002). Processing of IKONOS Imagery for sub-meter 3D positioning and building extraction. *ISPRS Journal of Photogrammetry & Remote Sensing, 56*(3):177-194.

Fraser, C., and H. B. Hanley (2003). Bias Compensation in Rational Functions for IKONOS Satellite Imagery. *Photogrammetry Engineering and Remote Sensing, 69*(1):53-57.

Fraser, C., and H. B. Hanley (2005). Bias compensated RPCs for sensor orientation of high-resolution satellite imagery. *Photogrammetric Engineering and Remote sensing, 71*(8):909-915.

Fraser, C.S., G. Dial and J. Grodecki (2006). Sensor orientation via RPCs. *ISPRS journal of Photogrammetry and Remote Sensing, 60*(3):182-194.

Grodecki, J., and G. Dial (2003). Block Adjustment of High-Resolution Satellite Images Described by Rational Polynomials. *Photogrammetry Engineering and Remote Sensing, Vol. 69*(1): 59-68.

Gruen, A., and L. Zhang (2002). Automatic DTM generation from Three-Line-Scanner (TLS) images. *GIT Kartdagar Symposium*, 17-19 April 2002, Stockholm. CDROM.

Hsia, J-S., and I. Newton (1999). A method for the automated production of digital terrain models using a combination of feature points, grid points, and filling back points. *Photogrammetric Engineering and Remote Sensing*, 65(6), pp. 713-719.

Hu, X., and C. V. Tao (2003). Automatic extraction of main-road centerlines from IKONOS and QuickBird imagery using perceptual grouping. Proc. of ASPRS 2003 Conference, Anchorage, Alaska, May 5-9. CDROM.

Jacobsen K. (2003). Geometric potential of IKONOS- and QuickBird-images. In D. Fritsch (Ed.) *Photogrammetric Weeks '03*, pp. 101-110.

Krauss, T., P. Reinartz, M. Lehner, M. Schroeder, and U. Stilla (2005). DEM generation from very high resolution stereo satellite data in urban areas using dynamic programming. *ISPRS Hannover Workshop 2005 on "High-Resolution Earth Imaging for Geospatial Information"*, Hannover, Germany, 17-20, May. CDROM.

Poli, D., L. Zhang, and A. Gruen (2004). SPOT-5/HRS stereo image orientation and automatic DSM generation. *IAPRSSIS, 35*(B1): 421-232.

Poon, J., C. Fraser, C. Zhang, L. Zhang, and A. Gruen (2005). Quality Assessment of Digital Surface Models Generated from IKONOS Imagery. *Photogrammetric Record, 20*(110):162-171.

Poon, J., C. Fraser, and C. Zhang (2007). Digital surface models from high resolution satellite imagery. *Photogrammetric Engineering and Remote Sensing*, In press.

Sohn, H., C. Park and H. Chang (2005). Rational function model-based image matching for digital elevation models. *Photogrammetric Record, 20*(112):366-383.

Toutin, T. (2004). Comparison of stereo-extracted DTM from different high-resolution sensors: SPOT-5, EROS-A, IKONOS-II, and QuickBird. *IEEE Transactions on Geoscience and Remote Sensing, 42*(10):2121-2129.

Zhang, C., and E. P. Baltsavias (2000). Knowledge-based image analysis for 3-D edge extraction and road reconstruction. *International Archives of the Photogrammetry, Remote Sensing and Spatial Information Sciences*, 33(B3/1): 1008-1015.

Zhang, C. (2003). Towards an operational system for automated updating of road databases by integration of imagery and geodata. *ISPRS Journal of Photogrammetry and Remote Sensing, 58*(3-4), 166-186.

Zhang, C., and C. Fraser (2007). Automated registration of high-resolution satellite images. *Photogrammetric Record, 22*(117):1-13.

Zhang, C., E. P. Baltsavias, and L. Sullivan (2005). Performance evaluation of ATOMI system for road database updating from aerial film, ADS40, IKONOS and Quickbird orthoimagery. *International Archives of Photogrammetry and Remote Sensing*, 29-30 August, Vienna, Austria. CDROM.

Zhang, L. and A. Gruen (2004). Automatic DSM generation from linear array imagery data. *International Archives of the Photogrammetry, Remote Sensing and Spatial Information Sciences*, 35(B3): 128-133.

Zhang, L. (2005). Automatic Digital Surface Model (DSM) Generation from linear array images. *Ph.D. Dissertation, Report No. 88*, Institute of Geodesy and Photogrammetry, ETH Zurich, Switzerland.

Zhang, L., and A. Gruen (2006). Multi-Image Matching for DSM Generation from IKONOS Imagery. *ISPRS Journal of Photogrammetry and Remote Sensing*, *60*(3), 195-211.